Constant Velocity Flying Spot for the estimation of in-plane thermal diffusivity on anisotropic materials

L. Gaverina, M. Bensalem, A. Bedoya, J. González, A. Sommier, J.L. Battaglia, A. Salazar, A. Mendioroz, A. Oleaga, J.C. Batsale, et al.

Constant Velocity Flying Spot for the estimation of in-plane thermal diffusivity on anisotropic materials

L. Gaverina [a], M. Bensalem [a], A. Bedoya [b], J. González [b], A. Sommier [a], J.L. Battaglia [a], A. Salazar [b], A. Mendioroz [b], A. Oleaga [b], J.C. Batsale [a] and C. Pradere [a,c 1]

[a] I2M-TREFLE, UMR CNRS 5295, Esplanade des Arts et Métiers 33405 Talence Cedex, France.

[b] Departamento de Física Aplicada I, Escuela de Ingeniería de Bilbao, Universidad del País Vasco UPV/EHU, Plaza Ingeniero Torres Quevedo 1, 48013 Bilbao, Spain.

[c] Tomsk Polytechnic University, Lenin Ave, 30, Tomsk, 634050, Russia.

Abstract

The Flying-Spot infrared thermography was introduced more than twenty years ago to detect narrow cracks. Recent progress made in optical control, lasers and infrared cameras allows extending the Flying-Spot technique for a quantitative thermal analysis. In this work, we propose a Constant Velocity Flying Spot to measure the in-plane thermal diffusivity of isotropic and anisotropic materials. We demonstrate that the logarithmic temperature profiles perpendicular to the laser motion are parabolic functions from which the thermal diffusivity along this direction is obtained. We have investigated two equivalent experimental configurations: (a) Moving laser with motionless sample and (b) moving sample with motionless laser spot. Both are of practical interest: the first one leads to identify thermal heterogeneities in macroscopic samples and the second one leads to measure the thermal properties of materials in in-line production processes. Measurements performed on calibrated samples (from insulators to good thermal conductors) with both configurations confirm the reliability of the method to measure the in-plane thermal diffusivity with an error less than 4 %.

[1] Corresponding author. Email: christophe.pradere@.u-bordeaux.fr

1. Introduction

Photohermal infrared thermography is an efficient tool to characterize the thermal diffusivity of solids. The flash method, both in the rear-face [1] and in the front-face [2] configurations, is a well-established technique for measuring the in-depth thermal diffusivity. In this method, a flat flash beam illuminates the whole sample surface homogeneously. Measuring the in-plane thermal diffusivity, instead, requires generating a thermal gradient along the surface. To do this, several illumination schemes have been proposed: a Gaussian spot [3-9], an annular area [10-12], a line or a strip [13-15] and a grid-like mask [16]. Measurements can be performed in the time-domain (pulsed excitation) or in the frequency-domain (modulated excitation).

In the nineties, with the aim of studying large surfaces in short times, it was introduced the so-called Flying-Spot infrared thermography. It consists in heating the sample surface with a moving continuous wave (cw)-laser spot and detecting the surface temperature field with an infrared video camera [17,18]. Since then, this technique has been developed and is suitable for the detection of defects, mainly vertical cracks, in a very fast and efficient way [19-27].

When an extremely short laser pulse heats the sample surface of a motionless isotropic and opaque material, the surface isothermals are concentric circles at all subsequent times. In a recent paper [9], authors demonstrated that the in-plane transient temperature profiles in natural logarithmic scale, Log(T), are parabolas and that the inverse of the second order coefficient of these parabolas behaves linearly as a function of time, the slope being directly related to the thermal diffusivity. This linear relation provides an excellent method to measure the thermal diffusivity in a fast and accurate way. The main advantage of this technique is that identifying the second order coefficient of the parabolas requires only few pixels around the heating spot.

In this work, we propose a method to measure the in-plane thermal diffusivity of opaque, isotropic and anisotropic samples based on the so-called Constant Velocity Flying Spot (CVFS), when a cw-laser spot is moving at a constant velocity along a straight line at the sample surface. In this case, increasing the motion speed leads to enhance the asymmetry of the surface temperature field. However, we will demonstrate that the transverse profiles of Log(T) with respect to the direction of the laser motion are still parabola and that the inverse of the second order coefficient of these parabola is a linear function of the distance to the laser

spot. From the slope of this straight line, the thermal diffusivity along the direction perpendicular to the laser motion can be derived easily.

It is worth writing that this method is also valid when the laser spot is motionless and the sample is moving at a constant velocity. This last configuration is of practical interest since it allows measuring the thermal diffusivity in in-line production processes, where heterogeneities, i.e. local changes in the thermal properties, can be detected in real time with a processing time less than 1 s on a I7 core with 128 Go of RAM computer.

To check the ability of the method to measure the thermal diffusivity efficiently using the CVFS, two experimental configurations have been designed. In the first one (Conf I), the sample is motionless while the laser is moving at constant velocity. In the second one (Conf II), the laser is motionless while the sample is moving at a constant velocity. In both cases (Conf I and II) the sensor (IR camera) is motionless. In-plane thermal diffusivity measurements performed in both configurations using calibrated samples covering a wide range of thermal diffusivities (from insulators to good thermal conductors) confirm the reliability of the method.

2. Material and experimental methods

2.1 Setups

Figure 1a and Figure 1b represent the Conf I (Motionless sample and moving laser). A cw laser diode (976 nm, 330 mW) is used to heat the surface of a sample. A Dual-Axis Scanning Galvo System (Thorlabs GVS112/M) is used to control the displacement of the laser spot at a constant velocity over the surface. A 160 mm focal length lens is used to reduce the spot diameter at 25 µm on the surface. With such a focal length, the scanning area is a (11 × 11) cm square and minimum displacement is 4.5 µm. A dichroic mirror, treated to reflect 95% of the visible light from 700 nm to 1000 nm and to transmit 95% of the infrared radiation between 2 and 16 µm, is used to direct the laser beam perpendicularly to the sample surface. The radiative emission of the sample surface is recorded by an IR video camera (FLIR SC7000, 320 × 256 pixels, pitch 30 µm, spectral band from 7 to 14 µm) equipped with a 25 mm focal length lens, which provides a spatial resolution of 250 ± 4 µm per pixel. More details on the setup can be found in Ref. [9].

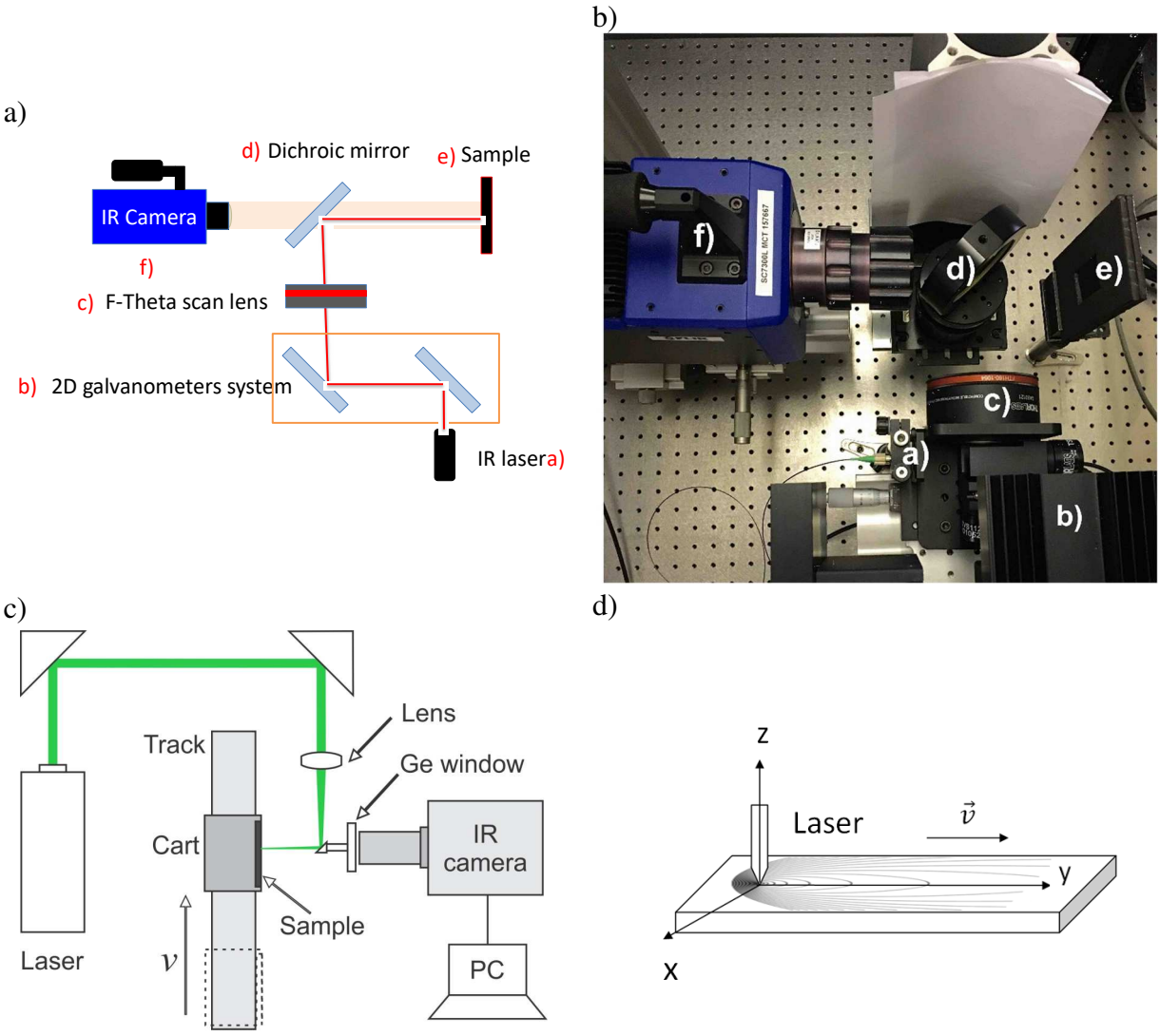

Figure 1: Experimental setup (developed at I2M lab) with a moving laser spot: a) sketch of the system and b) photo from the top. Experimental setup (developed at DFA) with a moving sample: c) sketch of the system and d) laser at fixed position and moving sample at constant velocity.

In the second setup Conf II (motionless laser spot and moving sample), which was developed at the Photothermal Techniques Laboratory in Bilbao, the laser spot is motionless and the sample is moved at constant velocity. The sketch of the experiment is shown in Figure 1c and Figure 1d. A cw laser (532 nm, up to 6 W) is directed by means of several mirrors and it is focused on the sample surface by a 10 cm focal length lens down to a radius of about 150 µm. A Ge window, which reflects visible light and transmits the IR wavelength, is used as a visible light filter for the camera. A small mirror, glued to the Ge window, allows the laser

beam to impinge the sample surface perpendicularly. An IR video camera (FLIR, model SC7500, 320×256 pixels, pitch 30 μm, spectral band from 3 to 5 μm) records the temperature field at the sample surface when it moves at a constant speed, *v*. An IR microscope lens is used to improve the spatial resolution of the IR camera down to 30 μm, with a field of view of 9.60 mm x 7.68 mm. The sample is mounted on a dynamic system (cart + track) that is coupled to an electronic system to control the speed of the cart between 2.5 and 10 $cm.s^{-1}$.

2.2 Constant Velocity Flying Spot (CVFS) methods

Regarding the setup of the Bilbao research group Conf II (motionless laser spot and moving sample), the speed of the sample is measured by counting the number of frames between the entrance and the exit of one end of the sample in the field of view of the camera and taking into account the length of the sample and the frame rate of the camera. In this way, the sample speed is measured with an uncertainty of less than 0.5%. We worked at the maximum frame rate allowed by the IR camera: 330 frames/s at full frame and up to 2000 frames/s applying a sub-windowing (320×70 pixels) with an integration time of 800 μs. On the other hand, in order to enhance the signal to noise ratio, several hundred of thermograms are averaged after reaching the steady state. For a comparison, we show in Figure 2 the single thermogram and the average thermogram corresponding to a Ni sample moving along the horizontal axis at 6 $cm.s^{-1}$. As can be observed, the noise reduction is remarkable and using this averaged thermogram the sample thermal diffusivity will be obtained with high accuracy, as it will be shown in section 5.

a) b)

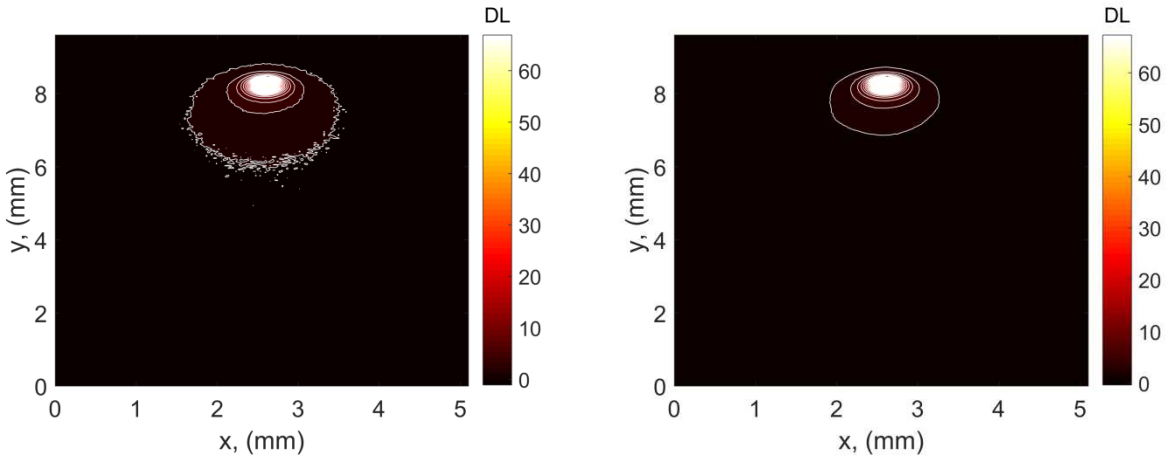

Figure 2: (a) Single thermogram and (b) averaged thermogram over several hundreds of thermograms corresponding to a Nickel sample moving downwards at 6 cm.s^{-1}.

Due to the versatility of the galvanometric system, an infinite number of different shapes could be generated for the laser displacement. In this study, a line is applied for the spot motion.

To understand the measurement ability, an example of CVFS realized on a PVC sample is represented in Figure 2.a. according to the following experimental conditions: (i), continuous laser beam with 6 mm.s^{-1} velocity, (ii) the diameter of the focused laser beam equal to d = 25 µm, (iii), power of 330 mW. While the parameters for the acquisition of the temperature fields are: (i), the spatial resolution of a pixel of the infrared camera is fixed at 250 ± 4 µm per pixel, (ii) the acquisition frequency of the camera is set at 200 Hz, (iii) the integration time is taken to be 500 µs, and (iv) acquisition takes place over a period of t = 5.3 s, representing 1050 images.

As illustrated in Figure 3, the laser beam scans the sample surface at constant speed as function of time along the y axis. As a first step, it is interesting to note the quality of the measurements with low noise levels. From these measurements, the scanning speed is determined by direct analysis of the measured temperature fields. For this purpose, an average of the film is produced in the direction x as illustrated in Figure 4. This makes it possible to obtain an image $I(y,t)$ for which it is possible to estimate the average speed of the laser. This image depicted in Figure 4.a shows the great regularity of the displacement due to the homogeneity and isotropic properties of PVC sample. From this space-time image, the maxima of each of the lines are extracted as well as their corresponding times. These points

are shown in Figure 4.b in order to determine the speed. In this example, a speed of about 6 $mm.s^{-1}$ is obtained.

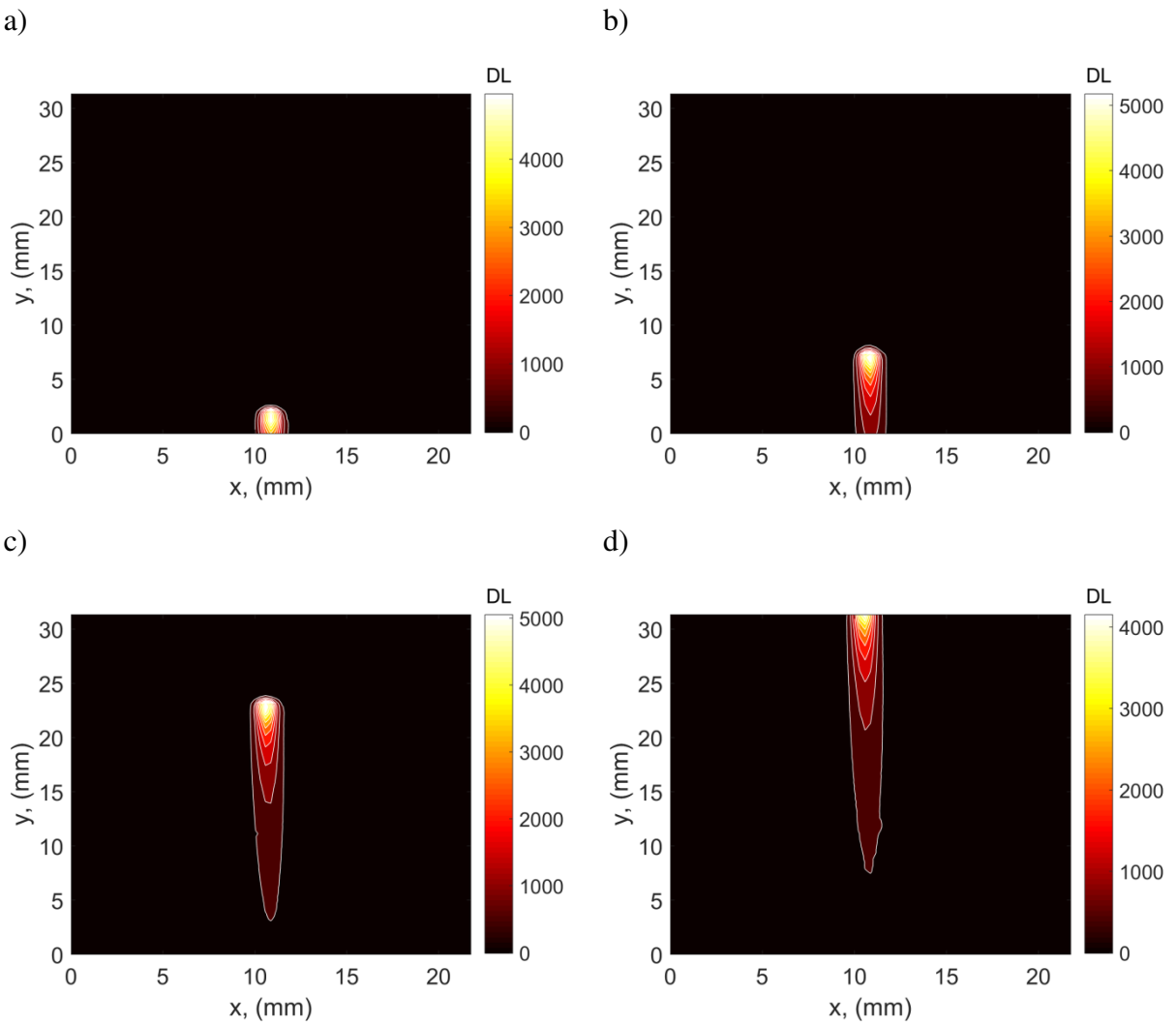

Figure 3: Excitation at constant scanning speed and with the laser continuously lit in the camera reference: a), temperature field at t = 0 s, b), temperature field after at t = 1.25 s, c), temperature field at t = 3.7 s and d) temperature field after completion of the sweep at t = 5.3 s.

a) b)

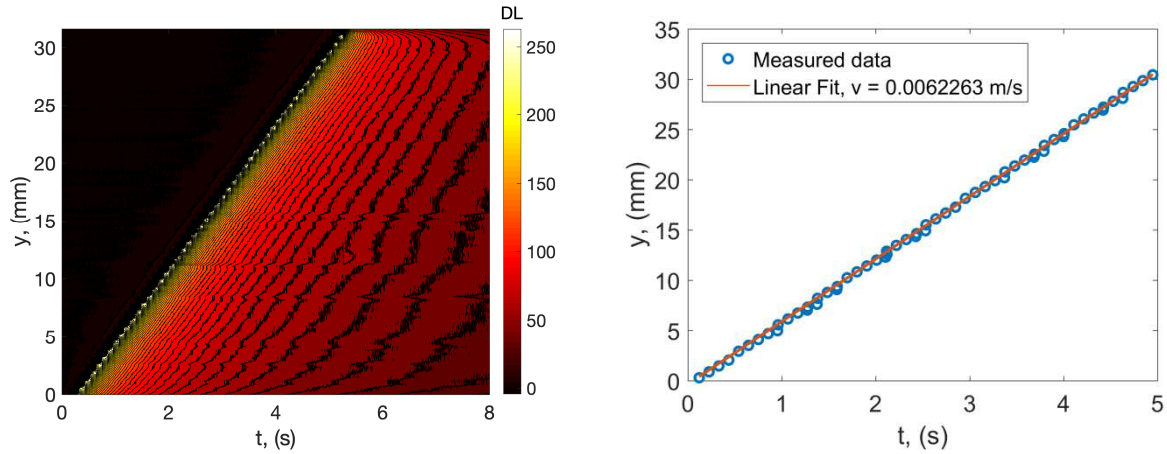

Figure 4: a), Image $I(y,t)$ of the mean of the film $T(x,y,t)$ made in the x direction and b), points representing the maxima according to y traced as a function of time for the estimation of the velocity of the laser beam.

From the knowledge of the average velocity of the laser scan, a change of mark can be performed (according to the processing method depicted in section 3.2) and represented Figure 5. This step consists in an interpolation of the temperature field from space and time representation $T(x,y,t)$ to space temperature $T(x,y)$ corresponding to the one of the laser once the steady state has been reached.

a) b)

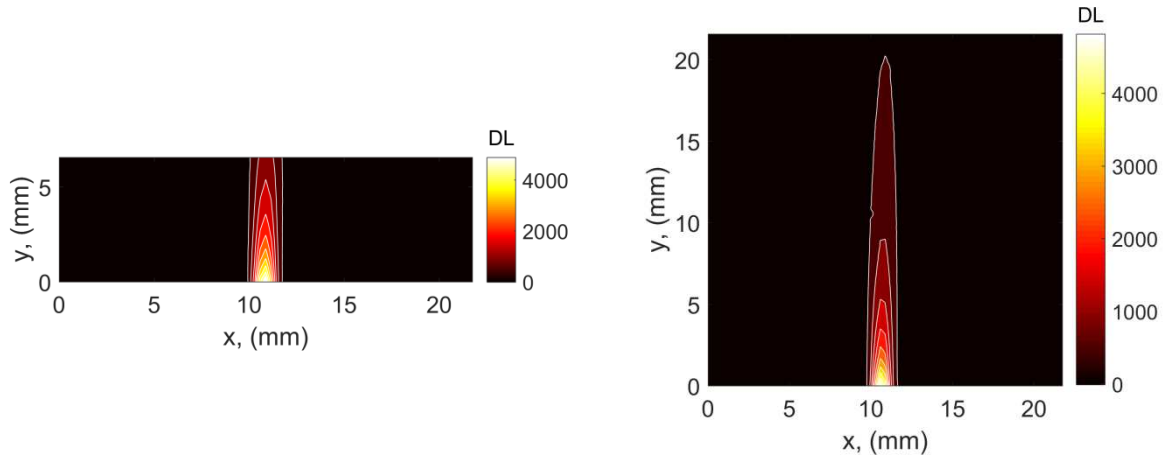

Figure 5: Excitation at constant scanning speed and with the laser continuously lit in the laser spot mark: a), temperature field after 6 mm of scanning, b), temperature field at the end of scanning.

2.3 Analysis of velocity and frequency dependencies

Observations from Figure 5 allow introducing the effect of both the laser velocity and the acquisition frequency from the IR camera. Depending on the value of these two parameters the reconstructed 2D spatial fields would be different. Increasing the acquisition frequency will increase the number of the acquired images. In such a case, the velocity of the laser spot will not be affected whereas the spatial resolution will be increased. To illustrate this fact, the estimated velocity, corresponding to the following cases: (i), continuous laser beam, (ii) the diameter of the focused laser beam equal to d = 25 µm, (iii), power of 330 mW, while the parameters for the acquisition of the temperature fields are: (i), the spatial resolution of a pixel of the infrared camera is fixed at 250 µm (with an uncertainty of ± 4 µm) per pixel, (ii) the acquisition frequency of the camera is set between 25 to 629 Hz, (iii) the integration time is taken to be 500 µs are represented in Figure 6.

a) b)

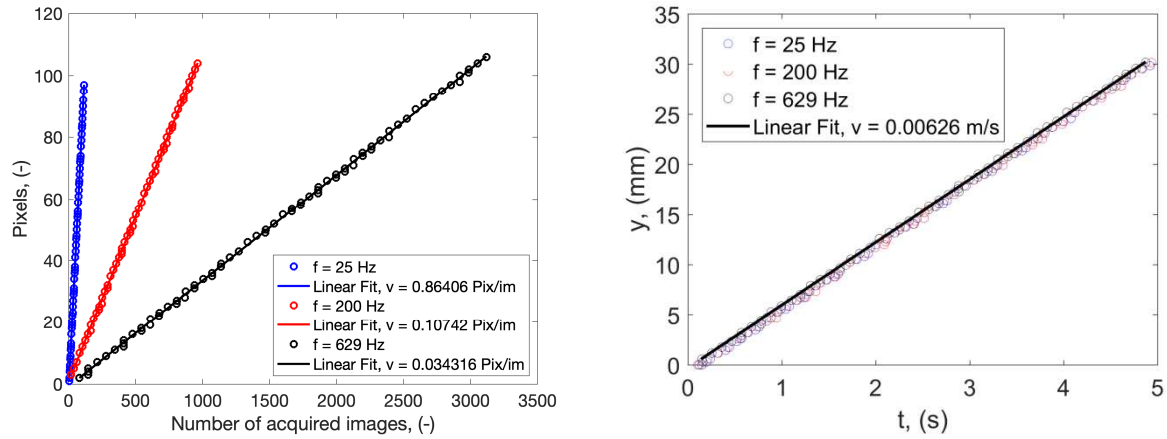

Figure 6: Laser displacement at constant velocity for different camera acquisition rates: a), displacement in pixel as function of number of images and b), displacement in mm as function of time.

To conclude it is important to notice that increasing the acquisition frequency is a way to increase the spatial resolution of the measurements when using a change of mark from the one of the camera image to the one of the laser spot. This is particularly easy due to the very high control or accuracy of the laser velocity.

2.4 Materials

Measurements will be performed on the samples presented in Figure 7. This sample panel is composed of several isotropic and anisotropic materials going from thermal conductors to insulators. The sample in Figure 7.a is an isotropic and insulating 15 cm × 15 cm Plexiglas plate. The one in Figure 7.b is an orthotropic 12 cm × 14 cm carbon / epoxy plate elaborated with fibres oriented along one direction. The one in Figure 7.c is a 9 cm × 3 cm Zinc plate. The thickness of each sample is not the same, but in this study, where the experimentation is performed in the front face, it has no influence on the modelization of the proposed method and the experimental results.

a) b) c)

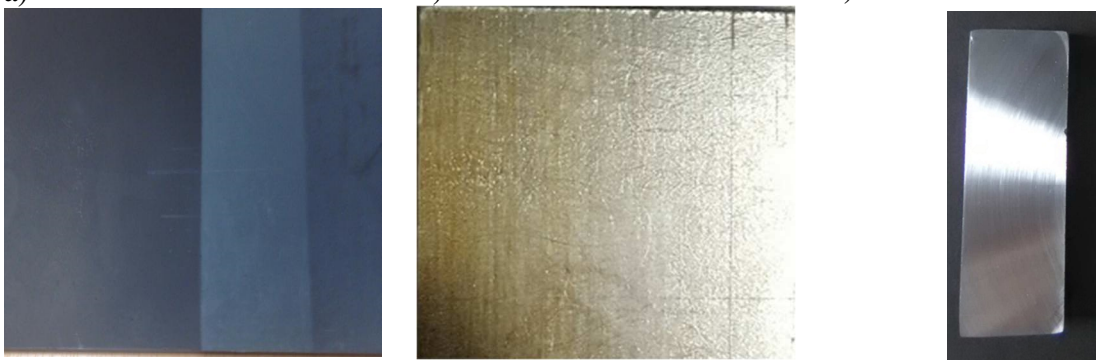

Figure 7: Sample to characterize: a) isotropic Polyethylene, b) anisotropic carbon / epoxy composite with fibres oriented along the vertical direction and c) isotropic Nickel.

3. Thermal modelization of the Constant Velocity Flying Spot (CVFS)

3.1 Transient thermal problem in the mark of the camera

Let us start considering an anisotropic, opaque and semi-infinite sample illuminated by an extremely brief (Dirac) pulse laser of Gaussian laser beam of radius b (at $1/e^2$). We make the Cartesian reference frame coincide with the principal axes of this anisotropic slab. The geometry of the problem is illustrated in Figure 8.

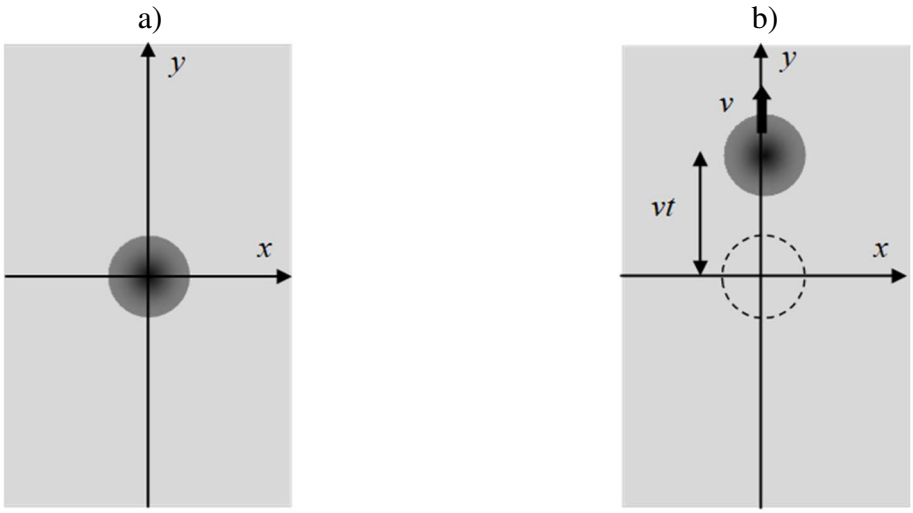

Figure 8: Front surface of an anisotropic sample illuminated by a Gaussian laser beam. a), the laser spot is at rest, centered at the origin and b), the laser spot is moving to the right at constant velocity *v*. It was switched on when it was at the origin (dotted circle).

In the absence of heat losses and for an infinite medium in z direction, the temperature rise above the ambient at the sample surface is given by [8]:

$$T(x,y,0,t)=\frac{2Q_o\eta}{\pi E_{zz}}\frac{1}{\sqrt{\pi t}}\frac{\exp\left(-\dfrac{2x^2}{b^2+8a_{xx}t}\right)}{\sqrt{b^2+8a_{xx}t}}\frac{\exp\left(-\dfrac{2y^2}{b^2+8a_{yy}t}\right)}{\sqrt{b^2+8a_{yy}t}} \tag{1}$$

Here Q_o is the energy of the laser pulse, η is the energy fraction absorbed by the sample, a is the thermal diffusivity and E is the thermal effusivity. Subscripts xx, yy, zz stand for the thermal properties along the principal axes.

If the laser spot is displaced a distance l to the right, along the principal axis y, and we deposit a small amount of energy dQ_o, then, following Eq. (1), the temperature is given by:

$$dT(x,y,0,t)=\frac{2}{\pi E_{zz}}\frac{1}{\sqrt{\pi t}}\frac{\exp\left(-\dfrac{2x^2}{b^2+8a_{xx}t}\right)}{\sqrt{b^2+8a_{xx}t}}\frac{\exp\left(-\dfrac{2(y-l)^2}{b^2+8a_{yy}t}\right)}{\sqrt{b^2+8a_{yy}t}}\eta dQ_o \tag{2}$$

Now we consider a cw laser of power P_o and Gaussian profile of radius b (at $1/e^2$) moving to the right at constant velocity v. The laser is switched on at $t = 0$, when it is at the origin of coordinates. The energy delivered by this laser in a short time dt is dQ_o = P_odt. The surface

temperature at time t, when the laser is at a distance $y = vt$, is given by the convolution integral (see Figure 8.b)

$$T(x,y,0,t)=\frac{2P_o\eta}{\pi E_{zz}}\int_0^t \frac{1}{\sqrt{\pi(t-\tau)}}\frac{\exp\left(-\frac{2x^2}{b^2+8a_{xx}(t-\tau)}\right)}{\sqrt{b^2+8a_{xx}(t-\tau)}}\frac{\exp\left(-\frac{2(y-v\tau)^2}{b^2+8a_{yy}(t-\tau)}\right)}{\sqrt{b^2+8a_{yy}(t-\tau)}}d\tau \qquad (3)$$

This equation allows us to calculate the surface temperature field at any time t after the laser was switched on, in the reference frame of the sample as illustrated in Figure 9. Simulations have been performed for an isotropic sample with $a = 1.10^{-7}$ m^2.s^{-1} and the laser moving at $v = 6$ mm.s^{-1}, the power $P_0 = 300$ mW, $\eta = 1$, $e_{zz} = 538$ J.K^{-1}.m^{-2}.s$^{-1/2}$ et e = 100 µm.

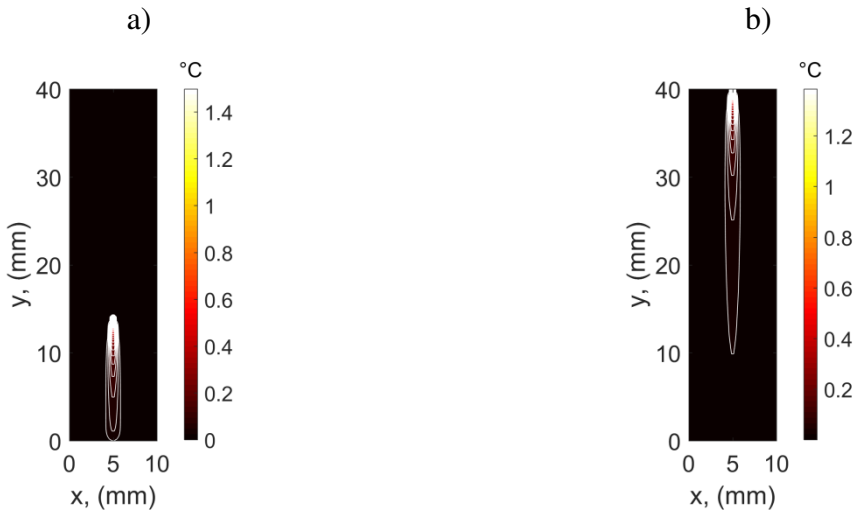

Figure 9: Excitation at constant scanning speed and with the laser continuously lit in the camera reference. a) Temperature field at t = 2 s, b), temperature field at t = 5.3 s.

3.2 Transient thermal problem in the mark of the Laser spot

If we are interested in measuring the thermal properties of a sample moving at constant velocity, we heat it with a laser beam, which remains at rest. To calculate the surface temperature in the laser mark we perform just a change in the reference frame in Eq. (3):

Let us consider the same anisotropic and infinite medium in z direction sample, as before moving to the left at constant velocity v, while the laser is at rest. The sample frame is (x,y,z) and the laser frame is (x',y',z'). The laser is switched on at $t = 0$, when both reference frames are superimposed (see Figure 10.a). At time t the sample is displaced to the left a distance $y' = -vt$ (see Figure 10.b).

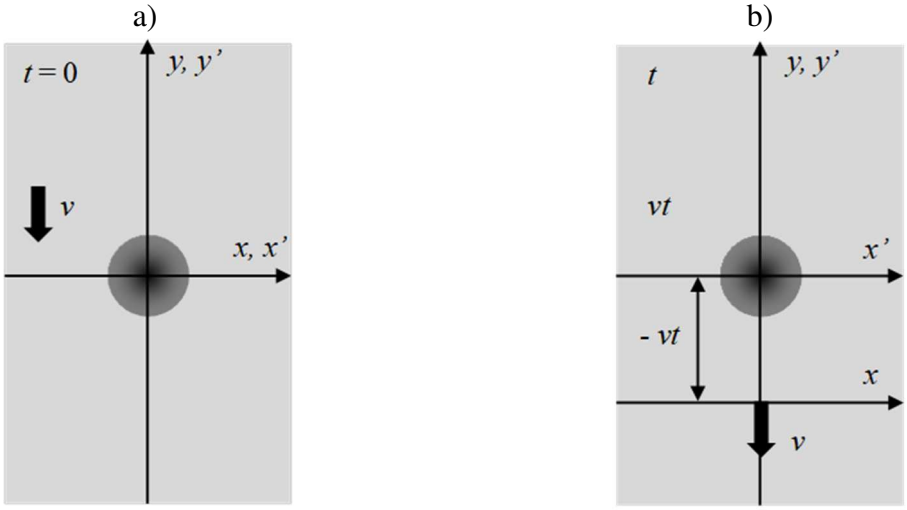

Figure 10: Front surface of an anisotropic sample moving to the left at constant velocity v, while the laser spot is at rest. a), The sample frame is (x,y,z) and the laser frame is (x',y',z') are superimposed at $t = 0$, when the laser was switched on and b), At time t the sample is displaced to the left a distance $y' = -vt$.

To calculate the temperature field in the laser frame we perform a change of coordinates since $y = y' + vt$. The exponentials in Eq. (3) can be transformed as $y - v\tau = y' + vt - v\tau = y' + v(t - \tau)$ and $x = x'$. Accordingly, the temperature in the laser frame is:

$$T(x', y', 0, t) = \frac{2P_o\eta}{\pi E_{zz}} \int_0^t \frac{1}{\sqrt{\pi(t-\tau)}} \frac{\exp\left(-\frac{2x'^2}{b^2 + 8a_{xx}(t-\tau)}\right)}{\sqrt{b^2 + 8a_{xx}(t-\tau)}} \frac{\exp\left(-\frac{2\left[y' + v(t-\tau)\right]^2}{b^2 + 8a_{yy}(t-\tau)}\right)}{\sqrt{b^2 + 8a_{yy}(t-\tau)}} d\tau \qquad (4)$$

It is worth mentioning that this problem was already solved by Gupta and co-workers for a moving isotropic fluid by solving the heat diffusion equation with a transport term [28].

From Eq. (4) the surface temperature field at any time t after the sample started moving can be calculated. Figure 11 shows the temperature fields at two different times after the sample started moving. Simulations have been performed for the same isotropic sample as in Figure 9, with $a = 1.10^{-7}$ m^2.s^{-1} and the sample moving at $v = 6$ mm.s^{-1}.

a) b)

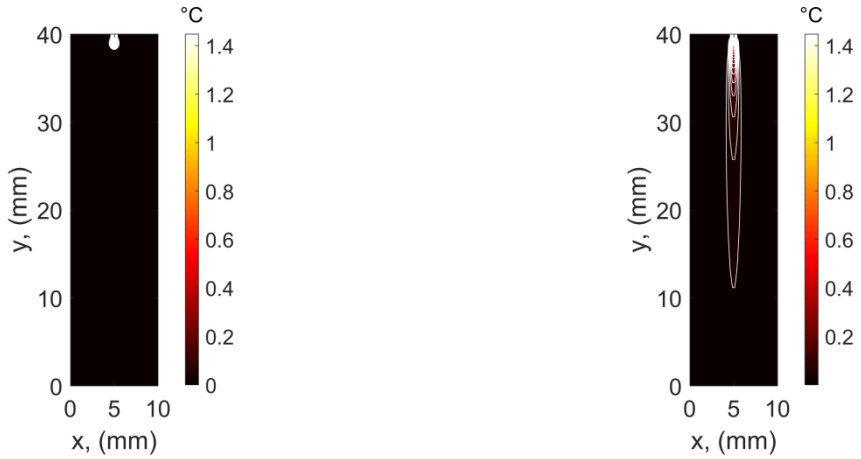

Figure 11: Excitation with the laser continuously lit and the sample moving at constant velocity. a) Temperature field at t = 0.2 s and (b) temperature field at t = 5.3 s.

According to the Relativity Principle, both Eq. (3) and Eq. (4) give the same temperature field. This result can be appreciated by comparing Figure 9b and Figure 11b, where the same thermogram is obtained regardless whether the laser or the sample is moving. Accordingly any procedure, moving the laser or moving the sample, can be used to retrieve the thermal transport properties of the sample. In Figure 12 we show the simulations of the natural logarithm of the temperature profiles in the direction perpendicular to the movement for the same material as in Figure 9 and Figure 11, when the steady state is reached. As can be observed, far away from the laser spot the temperature profiles look like parabolas. This result suggests the possibility of using the same method as in Ref. [9] for measuring the in-plane thermal diffusivity. However, Eqs. (3) and (4) are convolution integrals and it is difficult to develop an inverse procedure to retrieve the thermal diffusivity. That is the reason why we introduce in the next subsection a simplified theory to calculate the steady state temperature field if the heat diffusion along the laser movement direction is neglected. This assumption leads to an analytical expression of the surface temperature. It is worth mentioning that the validity of this simplified model increases with the laser speed and with the thermal diffusivity of the sample.

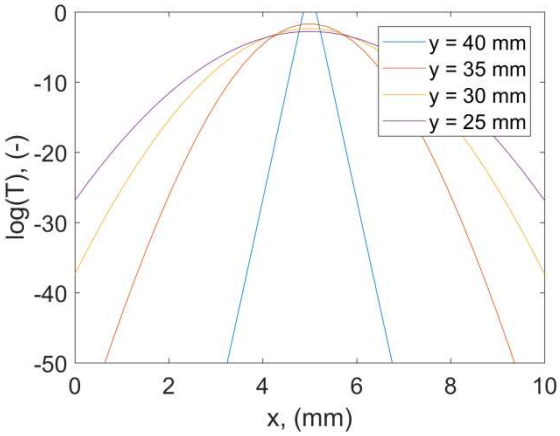

Figure 12: Logarithmic temperature profiles along the direction perpendicular to the laser movement (x) at several distances from the laser spot (y). Simulations have been performed for the same material and speed as in Figure 9 and Figure 11. The laser spot is centered at x = 5 mm and y = 40 mm.

3.3 Simplified model in stationary state

After having determined the scanning speed, the passage of the camera's reference mark (ie a transient 3D problem) to that of the laser beam (permanent 3D problem) is carried out and illustrated in Figure 5 and Figure 11 with respect to the principle of the scheme Figure 8 and Figure 10. This change of reference can be reflected in the equations in the form of a change of variable. This change of reference transforms the time variable t into the variable v/y where v is the laser beam velocity and y is the distance travelled by the latter.

With these considerations, the complete thermal problem could be written in steady state for a source point as follows:

$$\begin{cases} v_y \dfrac{\partial T_{vy}(x,y,z)}{\partial y} = a_{xx} \dfrac{\partial^2 T_{vy}(x,y,z)}{\partial x^2} + a_{zz} \dfrac{\partial^2 T_{vy}(x,y,z)}{\partial z^2} \\ T_{vy}(x, y=0, z) = 0 \\ -\dfrac{\partial T_{vy}(x,y,z)}{\partial x}\bigg|_{x=\pm l/2} = 0 \\ -\dfrac{\partial T_{vy}(x,y,z)}{\partial z}\bigg|_{z=0} = \dfrac{P_0}{\lambda_{zz}} \delta(x-x_0)\delta(y-y_0) \;;\; \dfrac{\partial T_{vy}(x,y,z)}{\partial z}\bigg|_{z=\to\infty} = 0 \end{cases} \tag{5}$$

Here a strong hypothesis is made assuming that the heat diffusion along the transport direction could be neglected. As a consequence, the term $a_{yy}\dfrac{\partial^2 T_{vy}(x,y,z)}{\partial y^2}$ is not taken into account to solve the thermal problem. This strong hypothesis is plausible when the velocity can be considered as important compared to the diffusion assuming that the Peclet number is larger than 10.

With the previous system of equations, a double Laplace and Fourier transforms can be applied to the system according to the following formulation:

$$\theta(\alpha_n, p, z) = \int_{x=-\frac{l}{2}}^{x=+\frac{l}{2}} \int_{y=0}^{y\to\infty} T_{vy}(x, y, z)\cos(\alpha_n x)\exp(-py)dxdy \tag{6}$$

By application of the boundaries conditions and the integral transformed equation (6) the solution in the transformed space is obtained:

$$\theta(\alpha_n, p, z) = \frac{P_0}{\lambda_{zz}\sqrt{\dfrac{a_{xx}}{a_{zz}}\alpha_n{}^2 + \dfrac{v_y p}{a_{zz}}}}\exp\left(-z\sqrt{\frac{a_{xx}}{a_{zz}}\alpha_n{}^2 + \frac{v_y p}{a_{zz}}}\right) \tag{7}$$

By using the inverse properties of the Laplace transformed (i.e. translation and scale properties), the expression of the temperature field in the real space is obtained:

$$T_{vy}(x, y, z) = \frac{P_0}{\rho C_p v_y}\frac{\exp\left(-\dfrac{v_y (x-x_0)^2}{4a_{xx}y}\right)}{\sqrt{\dfrac{\pi a_{xx} y}{v_y}}}\frac{\exp\left(-\dfrac{v_y z^2}{4a_{zz}y}\right)}{\sqrt{\dfrac{\pi a_{zz} y}{v_y}}} \tag{8}$$

where x_0 is the spatial coordinates of the laser spot versus x direction (m); a_{xx}, a_{zz} represent the thermal diffusivities versus the x and z directions ($m^2.s^{-1}$); P_0 is the power of the laser (W), and λ_{zz} corresponds to the thermal conductivity in z direction ($W.m^{-1}.K^{-1}$), and l (m) is the lateral dimension of the sample, v_y ($m.s^{-1}$) is the laser or sample velocity along y direction, ρ ($kg.m^{-3}$) is the mass density and C_p ($J.kg^{-1}.K^{-1}$) is the specific heat. Due to the experimental configuration, the measurements are performed at the surface of the sample (i.e. in z = 0), with this condition, the temperature is expressed by:

$$T_{vy}(x,y,z=0)=\frac{P_0}{\rho C_p v_y}\frac{\exp\left(-\frac{v_y\left(x-x_0\right)^2}{4a_{xx}y}\right)}{\sqrt{\frac{\pi a_{xx}y}{v_y}}\sqrt{\frac{\pi a_{zz}y}{v_y}}} \tag{9}$$

Here it is very important to notice that the solution equation (8) is also available when the CVFS is applied along the x direction. In that case, the complete problem could be solved and the new expression of the temperature is given by:

$$T_{vx}(x,y,z=0)=\frac{P_0}{\rho C_p v_x}\frac{\exp\left(-\frac{v_x\left(y-y_0\right)^2}{4a_{yy}x}\right)}{\sqrt{\frac{\pi a_{yy}x}{v_x}}\sqrt{\frac{\pi a_{zz}x}{v_x}}} \tag{10}$$

From an estimation point of view, it will be necessary to perform two kinds of thermal excitations: one along x and one along y directions to be able to estimate the thermal diffusivities along y and x directions. Finally, the following method should be used according to the direction of anisotropy of the sample. Future method based on the paper [10] would be addressed if an angle exists between the imaging axes and the orthotropic one.

4. Inverse processing

4.1 The Logarithmic Parabolic Method

The consideration of the spatial logarithm of the previous expressions (9) and (10) then yields the following expressions according to the x and y directions:

$$\begin{aligned}
&\log\left[T_{vy}(x,y,z=0)\right]=\log\left(\frac{k}{y}\right)-\frac{v_y\left(x-x_0\right)^2}{4a_{xx}y}\\
&\log\left[T_{vx}(x,y,z=0)\right]=\log\left(\frac{k}{x}\right)-\frac{v_x\left(y-y_0\right)^2}{4a_{yy}x}\\
&with\ k=\frac{P_0}{\pi\rho C_p\sqrt{a_{yy}}\sqrt{a_{zz}}}
\end{aligned} \tag{11}$$

The expression (11) can be used to obtain a polynomial relation of order 2 only as a function of the space x, y and the velocity v. This development reveals 3 coefficients function of v and ~~y~~ the spatial coordinate that must be estimated to determine the thermophysical properties of the problem. These properties will be estimated perpendicularly to the direction of the velocity term in other words of the scanning with the laser beam:

$$\begin{aligned}\log\left[T_{vy}(x,y,z=0)\right] &= \beta_{vy0}(y)+\beta_{vy1}(y)x+\beta_{vy2}(y)x^2\\ \log\left[T_{vx}(x,y,z=0)\right] &= \beta_{vx0}(x)+\beta_{vx1}(x)y+\beta_{vx2}(x)y^2\end{aligned} \tag{12}$$

with

$$\begin{cases}\beta_{vy2}(y)=-\dfrac{v_y}{4a_{xx}y}\ ;\ \beta_{vx2}(x)=-\dfrac{v_x}{4a_{yy}x}\\ \beta_{vy1}(y)=\dfrac{v_y x_0}{2a_{xx}y}\ ;\ \beta_{vx1}(x)=\dfrac{v_x y_0}{2a_{yy}x}\\ \beta_{vy0}(y)=-\dfrac{v_y {x_0}^2}{4a_{xx}y}+\log\left(\dfrac{k}{y}\right)\ ;\ \beta_{vx0}(x)=-\dfrac{v_x {y_0}^2}{4a_{yy}x}+\log\left(\dfrac{k}{x}\right)\end{cases} \tag{13}$$

Several comments arise from the previous expressions:

- β_2 is dependent only on the thermal diffusivities a_{xx} and a_{yy}. It is thus a suitable way to verify the in-plane homogenous transfer at different location, independent of the transverse heat transfer and the position of the spot.
- When the in-plane thermal diffusivities were estimated using β_2, the estimation of x_0 and y_0 could be conducted with the β_1 parameter or with the direct relation between β_1 and β_2.
- The estimation of β_0 is directly related to a 1D front face flash experiment. For example, the TSR method [6] could be used to estimate the parameter on an *log(T)* versus *log(x)* or *log(y)* graph representation and also take into account the heat losses.

4.2 Gauss-Markov inverse method

The inverse processing method consists in a linear least square method based on the logarithm of the temperature. The particularity of this method is to realize this inverse processing as function of the space and along the direction of the CVFS of the expressions (9) and (10). Nevertheless, the reconstructed spatial problem comes from the transient movie converted by using the method of section 3. For this reason, the noise of each pixel (i.e. spatial reconstruction of the temperature) is related to the noise associated to each pixel along time. Then, the measurement noise is considered uniform on the distribution and expressed as follows:

$$\widehat{T}(x, y, z=0) = T(x, y, z=0) + e_{T(x,y,z=0,t_i)} \tag{14}$$

where $e_{T(x,y,t_i)}$ is the random fluctuation added to a signal $T(x, y)$. It is considered to have a zero mean and uniform standard deviation (covariance matrix is diagonal). Moreover as the estimation could be performed along x or y directions linked to the main direction of the CVFS, the equation (14) can be rewritten as follow for each direction:

$$\begin{aligned} \widehat{T}_{vy}(x_i, y, z=0) &= T_{vy}(x_i, y, z=0) + e_{T(x_i,y,z=0)} \\ \widehat{T}_{vx}(x, y_i, z=0) &= T_{vx}(x, y_i, z=0) + e_{T(x,y_i,z=0)} \end{aligned} \tag{15}$$

where i represents the index of the variable corresponding to the direction of the CVFS. In agreement with the equation (12) a polynomial fitting can be implemented as function of the spaces x or y and the parameter β_n can be estimated by using a linear least-square relationship. It can be expressed as a linear combination of the logarithm of the measured temperature $\ln\left[\widehat{T}(x_i, y)\right]$ or $\ln\left[\widehat{T}(x, y_i)\right]$ as function of the parameter to estimate and the space variable as follow:

$$\begin{bmatrix} \log\left[\widehat{T}(x_1, y)\right] \\ \vdots \\ \log\left[\widehat{T}(x_N, y)\right] \end{bmatrix} = \begin{bmatrix} 1 & y_1 & {y_1}^2 \\ \vdots & \vdots & \vdots \\ 1 & y_M & {y_M}^2 \end{bmatrix} \begin{Bmatrix} \beta_{vx_i 0} \\ \beta_{vx_i 1} \\ \beta_{vx_i 2} \end{Bmatrix} \; for\ x\ direction$$
$$and \qquad (16)$$
$$\begin{bmatrix} \log\left[\widehat{T}(x, y_1)\right] \\ \vdots \\ \log\left[\widehat{T}(x, y_M)\right] \end{bmatrix} = \begin{bmatrix} 1 & x_1 & {x_1}^2 \\ \vdots & \vdots & \vdots \\ 1 & x_N & {x_N}^2 \end{bmatrix} \begin{Bmatrix} \beta_{vy_i 0} \\ \beta_{vy_i 1} \\ \beta_{vy_i 2} \end{Bmatrix} \; for\ y\ direction$$

The method of least squares assumes that there is constant variance in the noise, but in this case, the method of weighted least squares must be used because the ordinary least squares assumption of constant variance in the noise is violated (heteroscedasticity). The optimal estimation then yields:

$$\beta_{vx_i} = \left({S_y}^T W S_y\right)^{-1} {S_y}^T W \log\left[\widehat{T}(x_i, y)\right] \; along\ x\ direction$$
$$and \qquad (17)$$
$$\beta_{vy_i} = \left({S_x}^T W S_x\right)^{-1} {S_x}^T W \log\left[\widehat{T}(x, y_i)\right] \; along\ y\ direction$$

where W is given by the diagonal elements of the variance–covariance matrix in the noise and S_x and S_y the sensitivities matrix linked to the different space direction.

Finally, when the coefficients of the polynomial are estimated, a second linear Gauss-Markov method is applied between the estimated second order coefficient and the inverse of the distance (x or y) to realize a linear fit based on the relation (13) to retrieve the thermal diffusivity.

4.3 Validation of the inverse processing on analytical case

Even if the simplified proposed model is available in steady state and for high Peclet number, this formulation is not exact in terms of the true modelization of the complete problem depicted by equations (3) and (4). To study the error and bias of the simplified proposed model and inverse method, the two cases coming from the exact analytical solutions are minimized here.

First from the exact analytical method of Eq (3), where the laser is moving and the sample is at rest, the inverse processing depicted in section 4 is applied on the image case coming from Figure 9. The results relative to the parabolic fit of equation (12) are represented in Figure 13a for several positions. To point out the bias caused by the simplified proposed model and method, the residue of the fit is represented in Figure 13c. These residuals calculated as follow: $\varepsilon = 100\left(1 - \frac{\log\left(T(x, y_i, t_f\right)}{\beta_{vy0}(y) + \beta_{vy1}(y)x + \beta_{vy2}(y)x^2}\right)$ demonstrated that close to the laser spot, the bias is important with non-constant error and bias close to 5%. Whereas, far from the spot where the assumption of the model (steady state and high Peclet number) are satisfied, the residual are quite constant with value lower than 10^{-3}%. Finally, in Figure 13b, the linear fit between the second order of the estimated coefficients of the polynomial is represented. First, it is important to notice that close to the laser (where the model is biased) the linearity of the estimated data is not consistent. The same problem occurred very far where no thermal gradient subsists. Nevertheless, the estimation performed far from this border effects allows us to obtain an estimated thermal diffusivity of $9.89.10^{-8}$ m².s^{-1} for a true value of 1.10^{-7} m².s^{-1} meaning an error of 1.1%.

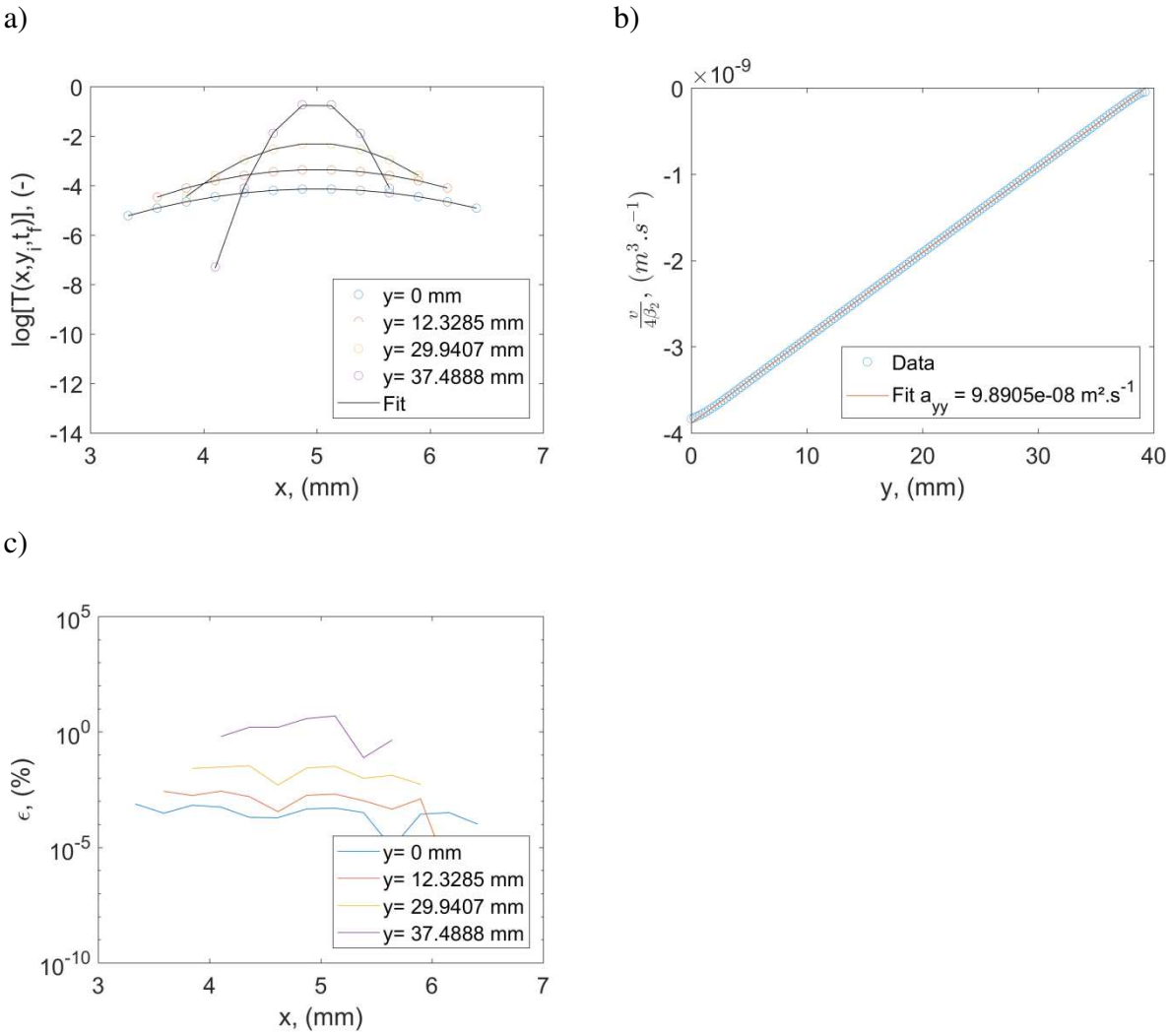

Figure 13: Validation of the proposed simplified method on exact analytical solution of equation (3): a), Parabolic fit of equation (12), b), linear fit of equation (13) and c), error ε of the parabolic approximation.

Secondly, from the exact analytical method of Eq (4), where the sample is moving and the laser is at rest, the inverse processing depicted in section 4 is applied on the image case coming from the Figure 11. The results relative to the parabolic fit to equation (12) are represented Figure 14.a for several positions. To point out the bias caused by the simplified proposed model and method, the residue of the fit is represented in Figure 14.c. These residuals demonstrate that close to the laser spot, the bias is important with non-constant error and bias~~ed~~ close to 5 %. Whereas, far from the spot where the assumptions of the model (steady state and high Peclet number) are satisfied, the residual are quite constant with value lower than 10^{-3} %. Finally, in Figure 14.b, the linear fit between the second order of the estimated coefficients of the polynomial is represented. First, it is important to notice that

close to the laser (where the model is biased) the linearity of the estimated data is not consistent. The same problem occurred very far where no thermal gradient subsists. Nevertheless, the estimation performed far from this border effects allows us to obtain an estimated thermal diffusivity of $9.95.10^{-8}$ m².s^{-1} for a true value of 1.10^{-7} m².s^{-1} meaning an error of 0.5%. Here it is important to notice that the change of mark previously depicted drastically increase the number of point (Figure 14.b) of the inverse processing. The consequence of this is a better spatial resolution and accurate estimation of the thermal diffusivity. Finally from an experimental point of view the uncertainty on the pixel size is around 1.5% and the one (see figure 6) on the velocity estimation is around 1%.

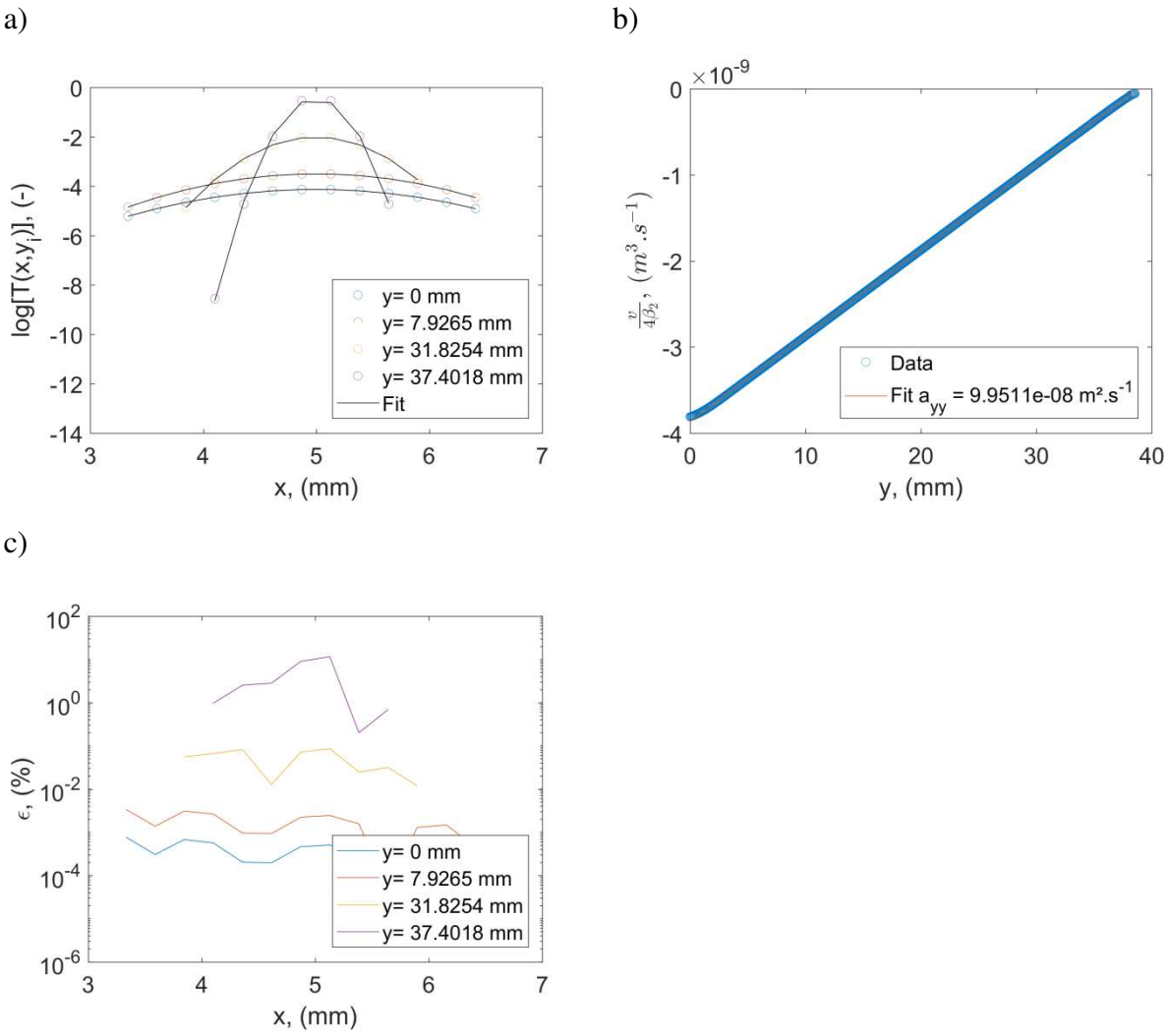

Figure 14: Validation of the proposed simplified method on exact analytical solution of equation (4): a), Parabolic fit of equation (12), b), linear fit of equation (13) and c), error ε of the parabolic approximation.

To conclude this part it is important to note that the proposed simplified model is precise enough to perform thermal diffusivity estimation based on CVFS technique with bias lower than 1 %. Note that this bias is not linked to the noise which will introduce more error.

5. Experimental results and discussion on homogeneous and orthotropic sample

To validate the parabolas method proposed in this work, we have measured a set of samples with calibrated thermal properties, covering a wide range from insulators to thermal conductors: Polyethylene, Polyether-ether-ketone (PEEK), stainless steel AISI-304, Ni and Zn. Moreover, a carbon / epoxy composite with the carbon fibres unidirectionally aligned has been studied to verify the ability of the method to characterize the thermal diffusivity of anisotropic samples. Both the Bordeaux setup, with the moving laser, and the Bilbao setup, with the moving sample, have been used.

As an example, we show in Figure 15 the results on Polyethylene using a moving laser (Conf I from Bordeaux team) at 8.5 $mm.s^{-1}$. Measurements have been performed in two orthogonal directions to verify the isotropy of the sample. Figure 15.a and Figure 15.b show the temperature fields, while Figure 15.c shows fittings of the parabolas. Finally, Figure 15.d shows the linear relation between the inverse of the second order coefficient of these parabolas and the longitudinal distance with respect to the laser spot. From the slope of these straight lines the thermal diffusivities along the two orthogonal directions are obtained according to the formula Eq (13): $a_{xx} = 1.48\times10^{-7}\ m^2.s^{-1}$ and $a_{yy} = 1.55\times10^{-7}\ m^2.s^{-1}$. Both results are very close, confirming the isotropy of the material, and in agreement with the literature value [30].

In Figure 16 we show the results on Ni using a moving sample (Conf II from Bilbao team) at 6.6 $cm.s^{-1}$. The retrieved thermal diffusivity is $a = 20.4\times10^{-6}\ m^2.s^{-1}$, which agrees with the literature value [30].

Finally, in Figure 17 we show the results for the carbon / epoxy composite (Conf I from Bordeaux team). Figure 17.a and Figure 17.b show a clear anisotropy in the temperature fields, i.e. heat propagates much longer along the x-axis, the direction of the carbon fibres. The retrieved thermal diffusivities confirm this thermal anisotropy: $a_{xx} = 3.53\times10^{-6}\ m^2.s^{-1}$ and $a_{yy} = 4.77\times10^{-7}\ m^2.s^{-1}$ (thermal anisotropic ratio of 7.4). These values are in good agreement

with the literature ones [9,10,31]. Table 1 summarizes all measurements performed in this work. Finally, the following method should be used according to the direction of anisotropy of the sample. Future method based on the paper [10] would be addressed if an angle exists between the imaging axes and the orthotropic one.

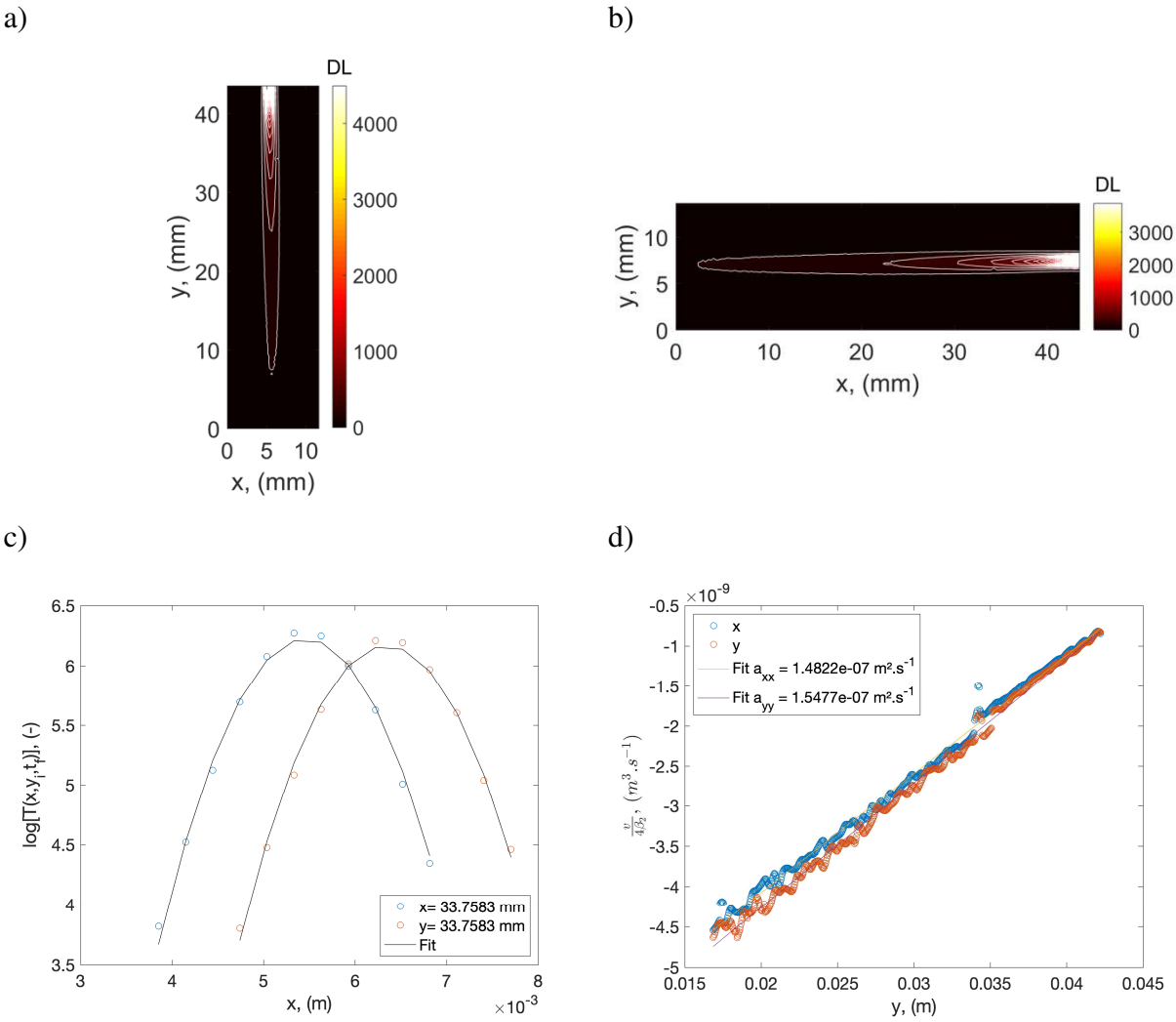

Figure 15: Measurement on Polyethylene sample: a) Reconstructed temperature field in the mark of the laser for the laser moving along y direction, b) reconstructed temperature field in the mark of the laser for the laser moving along x direction, c) example of parabolic fit along x direction (ie for the temperature field a)) and y direction (ie for the temperature field b) and d) linear fits along x and y directions.

Table 1. Retrieved thermal diffusivities ($\times 10^{-6}$ $m^2.s^{-1}$) values using the parabolas method. The uncertainty is less than 4 %.

Sample	Thermal diffusivity (moving laser)	Thermal diffusivity (moving sample)	Thermal diffusivity (Literature)[29-32]

Polyethylene	0.148-0.155		0.14-0.18
Carbon/epoxy ∥	3.53		3.8
Carbon/epoxy ⊥	0.48		0.45-0.64
PEEK		0.20	0.18
AISI-304		4.0	3.95
Ni		20.4	22
Zn		43	41.8

a) b)

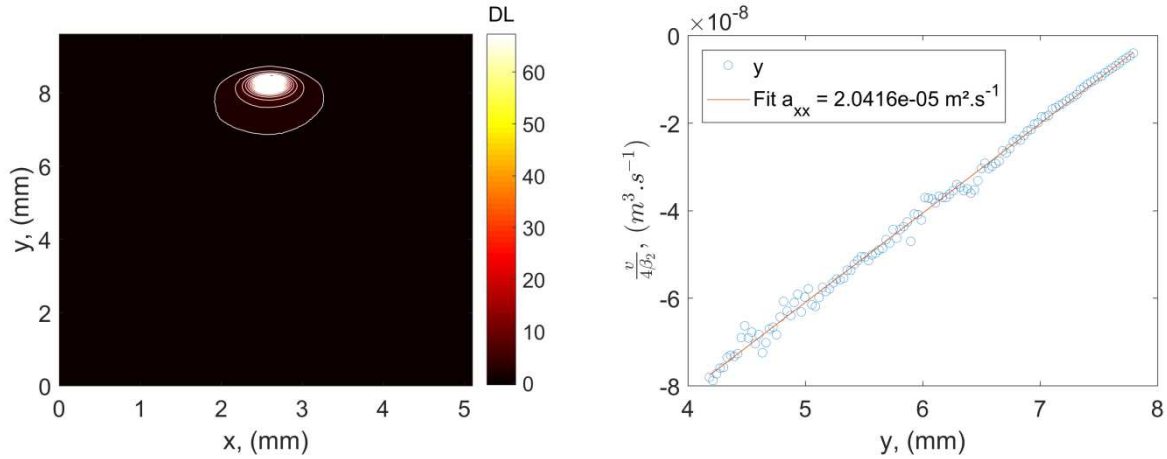

Figure 16: Measurement and method on Nickel sample at 6 cm.s^{-1}: a), Reconstructed temperature field in the mark of the laser for the sample moving along the y direction, b), linear fits along y direction.

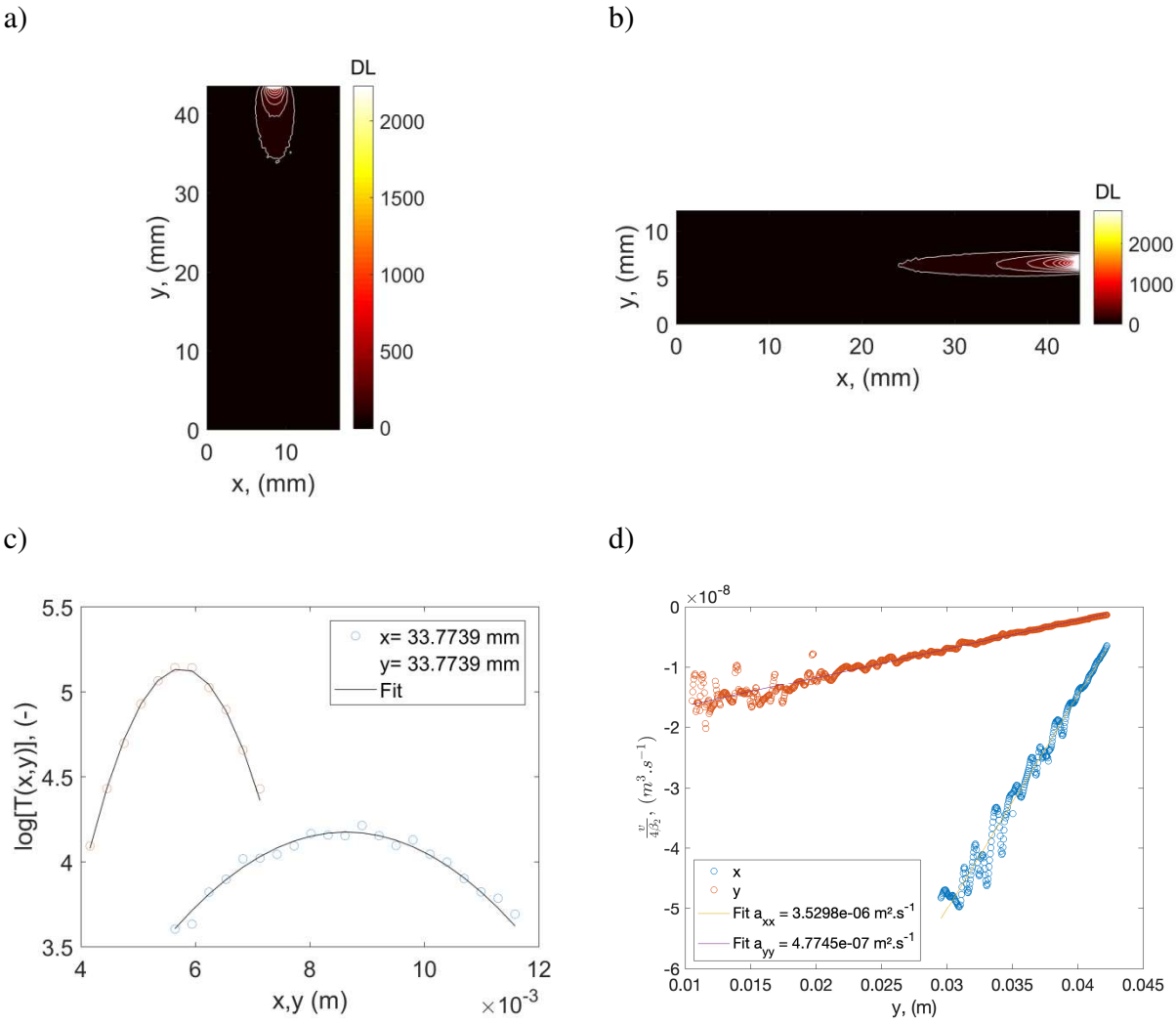

Figure 17: Measurement and method on 1D carbon / epoxy Composite sample at 8.5 mm.s^{-1}: a), Reconstructed temperature field in the mark of the laser for the laser moving along y direction, b), reconstructed temperature field in the mark of the laser for the laser moving along x direction, c), example of parabolic fit along x direction (ie for the temperature field a)) and y direction (ie for the temperature field b)) and (d), linear fits along x and y directions.

6. Conclusion

We propose a method to measure the in-plane thermal diffusivity of (an)isotropic samples using the Constant Velocity Flying Spot IR thermography, where a laser spot scans the sample surface along a straight line at constant speed. The method consists in studying the surface temperature field in logarithmic scale. Using a simplified model, which neglects heat propagation in the direction of the laser movement, we have demonstrated analytically that

the transverse profiles of Log(T) with respect to the laser movement are parabolas. The inverse of the second order coefficient of these parabolas depends linearly on the distance to the laser spot, its slope giving the thermal diffusivity. Moreover, according to the Relativity Principle, this method is also valid when the laser remains fixed in the camera mark while the sample is moving at constant velocity. Experimental measurements performed on a set of materials covering a wide range of diffusivity values confirm the validity of the method. This work opens the way to measure real time thermal diffusivity of samples in an industrial environment, e.g. covering big surfaces with a moving laser or analysing moving samples (in an in-line production) with a fixed laser. Another advantage is the ability of the method to characterize high thermal conductor sample by adjusting the scanning velocity in agreement with the camera acquisition rate.

Acknowledgments

This work was supported by “Projet Région Aquitaine”, by “Epsilon-Alcen” industrial group, by “Ministerio de Economía y Competitividad” (DPI2016-77719-R, AEI/FEDER, UE) and by “Universidad del País Vasco UPV/EHU” (GIU16/33).

References

[1] W.J. Parker, R.J. Jenkins, C.P. Butler and G.L. Abbott, Flash method of determining thermal diffusivity, heat capacity, and thermal conductivity, J. Appl. Phys. **32**, 1679-84 (1961).

[2] D.L. Balageas, Thermal diffusivity measurement by pulsed methods, High Temp.-High Press. **21**, 85-96 (1989).

[3] J.-C. Krapez, G. Gardette, Characterization of anisotropic materials by steady-state and modulated thermal ellipsometry, High Temp. High Press. **30**, 567 (1998).

[4] J.F. Bisson, D. Fournier, Influence of diffraction on low thermal diffusivity measurements with infrared photothermal microscopy, J. Appl. Phys. **83**, 1036 (1998).

[5] C.S. Welch, D.M. Heath, W.P. Winfree, Remote measurement of in-plane diffusivity components in plates, J. Appl. Phys. **61**, 895 (1987).

[6] F. Cernuschi, A. Russo, L. Lorenzoni, A. Figari, In-plane thermal diffusivity evaluation by infrared thermography, Rev. Sci. Instrum. **72**, 3988 (2001).

[7] P. Bison, F. Cernuschi and S. Capelli, A thermographic technique for the simultaneous estimation of in-plane and in-depth thermal diffusivities of TBCs, Surface & Coating Technology **205**, 3128 (2011).

[8] N.W. Pech-May, A. Mendioroz and A. Salazar, Simultaneous measurement of the in-plane and in-depth thermal diffusivity of solids using pulsed infrared thermography with focused illumination, NDT&E International **77**, 28-34 (2016).

[9] L. Gaverina, J.C. Batsale, A. Sommier and C. Pradere, Pulsed flying spot with the logarithmic parabolas method for the estimation of in-plane thermal diffusivity fields on heterogeneous and anisotropic materials, J. Appl. Phys. **121**, 115105 (2017).

[10] L. Gaverina, A. Sommier, J.L. Battaglia, J.C. Batsale and C. Pradere, Pulsed Flying Spot Elliptic method for the estimation of the thermal diffusivity field of orthotropic materials. Int. J. Therm. Sci. **125**, 142-148 (2018).

[11] D. Demange, P. Beauchene, M. Bejet, R. Casulleras, Mesure simultanée de la diffusivité thermique selon les deux directions principales d'un matériau, Rev. Gen. Therm. **36**, 755 (1997).

[12] P. Cielo, L.A. Utracki, M. Lamontagne, Thermal diffusivity measurements by the converging thermal wave technique, Canad. J. Phys. **64**, 1172 (1986).

[13] S. Alterowitz, G. Deutscher, M. Gerhenson, Heat capacity and thermal conductivity of sintered Al_2O_3 at low temperatures by the heat pulse technique, J. Appl. Phys. **46**, 3637 (1975).

[14] I. Philippi, J.C. Batsale, D. Maillet, A. Degiovanni, Measurement of thermal diffusivities through processing of infrared images, Rev. Sci. Instrum. **66**, 182 (1995).

[15] C. Welch, J. Johnson, Thermographic measurement of in-plane diffusivity in very thin plates using diffusion of thermal patterns, in: D.O. Thompson, D.E. Chimenti (Eds.), Rev. Progress in Quant. Nondestr. Eval., vol. 19, Plenum, New York, 1999, pp. 1449–1456.

[16] J.C. Krapez, L. Spagnolo, M. Frieb, H.P. Maier and G. Neuer, Measurement of in-plane diffusivity in non-homogeneous slabs by applying flash thermography, Int. J. Therm. Sci. **43**, 967 (2004).

[17] Y.Q. Wang, P.K. Kuo, L.D. Favro and R.L. Thomas, A novel "flying-spot" infrared camera for imaging very fast thermal-wave phenomena, In Photoacoustic and Photothermal Phenomena II Springer Series in Optical Sciences **62**, 24-26 (1990).

[18] C. Gruss and D. Balageas. Theoretical and experimental applications of the flying spot camera. Proc QIRT 92 Conference (Seminar Eurotherm No 27) D Balageas, G Busse, GM Carlomagno eds Editions Europennes Thermique et Industrie, Paris. 1992;:19–24. Available from: QIRT Open Archives: www.qirt.org/dynamique/index.php?idD=55, Paper QIRT 1992-004.

[19] J.L. Bodnar and M. Egée, Wear crack characterization by photothermal radiometry, Wear **196**, 54-59 (1996).

[20] J.C. Krapez, Résolution spatiale de la cemara thermique à source volante, Int. J. Therm. Sci. **38**, 769-779 (1999).

[21] J. Schlichting, M. Ziegler, A. Dey, Ch. Maierhofer and M. Kreutzbruck, Efficient data evaluation for thermographic crack detection, QIRT J. **8**, 119-123 (2011).

[22] S.E. Burrows, S. Dixon, S.G. Pickering, T. Li and D.P. Almond, Thermographic detection of surface breaking defects using a scanning laser source, NDT&E Int. **44**, 589-596 (2011).

[23] T. Maffren, P. Juncar, F. Lepoutre and G. Deban, Crack detection in high-pressure rurbine blades with flying spot active thermography in the SWIR range, Rev. Progress Quantitative Nondestructive Evaluation, AIP Conference Proc. **1430**, 515-522 (2012).

[24] U. Netzelmann, Flying-spot lock-in thermography and its application to thickness measurement and crack detection, QIRT Conference Bordeaux 2014. Available from: QIRT Open Archives: http://dx.doi.org/10.21611/qirt.2014.064.

[25] A. Thiam, J.C. Kneip, E. Cicala, Y. Caulier, J.M. Jouvard and S. Mattei, Modeling and optimization of open crack detection by flying spot thermography, NDT&E Int. **89**, 67-73 (2017).

[26] N. Montinaro, D. Cerniglia and G. Pitarresi, Detection and characterization of disbonds on fibre metal laminate hybrid composites by flying laser spot thermography, Composites Part B **108**, 164-173 (2017).

[27] C. Boué and S. Holé, Open crack depth sizing by multi-speed continuous laser stimulated lock-in thermography, Meas. Sci. Technol. **28**, 065901 (2017).

[28] Q. He, R. Vyas and R. Gupta, Theory of photothermal spectroscopy in an optically dense fluid, Appl. Opt. **36**, 1841-1846 (1997).

[29] Goodfellow catalogue at http://www.goodfellow.com.

[30] Y.A. Çengel, *Heat Transfer: A practical Approach* (McGraw-Hill, Boston, 2003).

[31] Thomas, M., Boyard, N., Lefèvre, N., Jarny, Y., & Delaunay, D. (2010). An experimental device for the simultaneous estimation of the thermal conductivity 3-D tensor and the specific heat of orthotropic composite materials. International Journal of Heat and Mass Transfer, 53(23), 5487-5498.

[32] L.R. Touloukian, R.W. Powell, C.Y. Ho and M.C. Nicolasu, *Thermal Diffusivity* (IFI/Plenum, New York , 1973).